Article ID: 1000-7032(2022)05-0633-09

Optimal Doping Content of Red Emitting $Y_4GeO_8:Bi^{3+},Eu^{3+}$ Phosphor Designed by Response Surface Methodology

XU Shu-jun, CHEN Jing, CHEN Li-yuan,
ASHRAF Ghulam-Abbas, LI Hui-jun, GUO Hai*
(*Department of Physics, Zhejiang Normal University, Jinhua* 321004, *China*)
* *Corresponding Author, E-mail: ghh@zjnu.cn*

Abstract: Herein, a more direct method, response surface methodology, is used to predict the strongest red emission of $Y_4GeO_8:Bi^{3+},Eu^{3+}$ samples. The concentrations of Bi^{3+} and Eu^{3+} of the optimal sample were predicted to be 31.03% and 67.36% (in mole ratio), respectively. The optimal sample was prepared and photoluminescent properties were measured and characterized. Y_4GeO_8: 31.03% Bi^{3+}, 67.36% Eu^{3+} has strongest red emission. The difference between the intensity of experimental value and theoretical value is very small. The color coordinate of the as-prepared sample is (0.645 7, 0.349 0), which is very close to the color coordinate of standard red light (0.670 0, 0.330 0). The luminous color of the sample is pure, and the calculated color purity reaches 98%. What's more, the internal quantum efficiency of the sample is as high as 72.5%. In a word, this paper provides an approach for searching the optimal doping concentration of phosphors with the strongest luminescence directly, which can be used in exploring all types of co-doped phosphors.

Key words: $Y_4GeO_8:Bi^{3+},Eu^{3+}$ phosphors; response surface methodology; luminescent intensity
CLC number: O482.31 **Document code**: A **DOI**: 10.37188/CJL.20220021

效应面优化模型获取 $Y_4GeO_8:Bi^{3+},Eu^{3+}$ 红色荧光粉掺杂浓度

徐淑君, 陈 静, 陈礼元, ASHRAF Ghulam-Abbas, 李慧军, 郭 海*
(浙江师范大学 物理系, 浙江 金华 321004)

摘要: 使用更直接的方法(效应面优化模型)预测了 $Y_4GeO_8:Bi^{3+},Eu^{3+}$ 样品的最强红光发射。预测最佳样品掺杂的 Bi^{3+} 离子和 Eu^{3+} 离子浓度分别为 31.03% 和 67.36%(摩尔分数)。制备最佳样品后对其光致发光性能进行了测试和表征。荧光粉 Y_4GeO_8: 31.03% Bi^{3+}, 67.36% Eu^{3+} 具有最强的红光发射,并且强度的实验值和理论值之间的差值很小。优化样品的色坐标为(0.645 7,0.349 0),计算出的色纯度为 98%,内量子效率高达 72.5%。本文提供了一种直接寻找发光最强的荧光粉最佳掺杂浓度的方法,可用于探索各种类型的共掺杂荧光粉。

关 键 词: $Y_4GeO_8:Bi^{3+},Eu^{3+}$ 荧光粉; 效应面优化模型; 发光强度

收稿日期: 2022-01-17; **修订日期**: 2022-02-07
基金项目: 国家自然科学基金(11974315)资助项目
Supported by National Natural Science Foundation of China(11974315)

1 Introduction

In the field of solid-state lighting, white light emitting diode (W-LED) has attracted extensive attention because of its high efficiency, no pollution and long service lifetime[1-4]. Generally, W-LED can be made of blue light chip and yellow phosphor, YAG:Ce^{3+}. However, the lack of red light leads to low color rendering index and high color temperature. In this regard, some researchers have proposed a feasible method for fabricating W-LED using ultraviolet (UV) chip and red, green and blue phosphors[5-6]. No matter which method is used to prepare W-LED, the red-light component is very important.

At present, some researchers are committed to exploring red phosphors[7-8]. For example, Yue *et al*. reported red-emitting $Sr_3La(AlO)_3(BO_3)_4$:Eu^{3+} phosphors with high color purity of 92.4%[9]. Guo *et al*. synthesized red-emitting $Na_3Sc_2(PO_4)$:Eu^{3+} phosphors with quantum efficiency of 49%[10]. Wang *et al*. prepared red-emitting Gd_2InSbO_7:Eu^{3+} phosphors with Commission Internationale de L'Eclairage (CIE) of (0.629 0, 0.371 0)[11]. All the red phosphors studied above have good luminescent properties. Usually, researchers change the concentration of doped ions by the control variable method to seek the strongest luminescence. But this traditional method cannot find the strongest luminescence directly. Therefore, some researchers want to explore whether there is a direct way to find the strongest luminescence. Some researchers have found that the response surface methodology (RSM) can be used to determine an optimal value of some problems. And RSM has the advantages, such as displaying the relationships between independent and dependent variables, including error analysis, and saving time and low cost[12-14]. For instance, Li *et al*. predicted the best conditions to reach the maximum relative density of calcia partially stabilized zirconia by RSM[15]. Luo *et al*. studied the effects of extraction temperature, extraction time, ratio of water and their interaction on the yield of urea dioxide total polysaccharide by RSM[16]. Theoretically, most of the methods are universal. In other words, RSM is also feasible in the field of luminescent materials.

Due to their stable properties and high solubility of rare earth ions, germanate phosphors have stimulated the interest of researchers in recent years[17-19]. For doped ions, Eu^{3+} is a very excellent activator for red emission, but its intensity is very weak[20-23]. It is necessary to introduce a sensitizer to enhance its luminous intensity[18]. Bi^{3+} is an excellent sensitizer[24-25]. The co-doping of Bi^{3+} and Eu^{3+} can improve the luminous intensity of phosphors[26-28]. Therefore, the phosphor Y_4GeO_8:Bi^{3+},Eu^{3+} was selected as an example to optimize by RSM.

The purpose of this study is to determine the optimal doping concentrations of Bi^{3+} and Eu^{3+} in Y_4GeO_8:Bi^{3+},Eu^{3+} phosphors through uniform design and RSM. Through simulation, the ions concentrations of Bi^{3+} and Eu^{3+} are 31.03% and 67.36% (in mole ratio), respectively. The CIE, color purity and quantum efficiency of Y_4GeO_8:31.03% Bi^{3+},67.36% Eu^{3+} phosphors were further studied. The color purity of the optimal sample is as high as 98%, and its internal quantum efficiency is 72.5%.

2 Experiments

2.1 Sample Preparation

A series of Y_4GeO_8:Bi^{3+},Eu^{3+} phosphors were synthesized by solid-state reaction method. Firstly, the basic materials Y_2O_3 (99.99%), GeO_2 (99.999%), Bi_2O_3 (99.99%), Eu_2O_3 (99.99%) and H_3BO_3 (99.8%) were weighed conforming to the stoichiometric ratio, in which H_3BO_3 was used as the cosolvent. Secondly, basic materials were ground in a mortar for 30 min. Alcohol was added during the grinding process to help the raw materials mix evenly. The uniformly blended material was then placed in an alumina crucible and sintered for 5 h at 1 400 ℃. Finally, after cooling, the sintered sample was ground into powder for further characterization.

2.2 Characterizations

X-ray diffraction (XRD) patterns were characterized by Rigaku MiniFlex/600 using Cu Kα1 radiation.

An Edinburgh FS5 spectrofluorometer with a 150 W Xe lamp was used to examine the samples' excitation and emission spectra. Samples with the same mass were added into the same sample holders. For spectra measurement, the position of the samples remains unchanged, and the spectrometer parameters remain unchanged for better comparison. Internal quantum efficiencies and temperature-dependent photoluminescence spectra were obtained using FS5 spectrofluorometer with a TCB1402C temperature controller(China) and a SC-30 integrating sphere, respectively.

2.3 Uniform Design and RSM

Uniform design can narrow the experimental range of RSM according to the experimental results. So $U_9(9^2)$ test table was used to design the experiment. RSM was used to determine the best combination of experimental parameters (concentrations of Bi^{3+} and Eu^{3+}) to obtain the strongest luminescence. RSM needs to be reflected in the coding space, so central composite design(CCD) was used to encode the experimental parameters. The data obtained by RSM were analyzed by variance, and the obtained data were judged by T-test and F-test. F-test was used to determine the credibility of the RSM's equation. T-test is used to determine whether the equation is loss of fitting[12-16].

3 Results and Discussion

3.1 Results and Analysis of Uniform Design

The $U_9(9^2)$ uniform design table is shown in Tab. 1. According to the results reported in the literature, the doping concentrations ranges of Bi^{3+} and Eu^{3+} ions are preliminarily selected as 10% – 60% and 20% – 120%, respectively[18]. Nine samples were uniformly designed according to $U_9(9^2)$, and the doping concentrations of Bi^{3+} and Eu^{3+} ions in each sample are located in column 2 and column 3 of Tab. 1, respectively. The integrated intensities of photoluminescence(PL) spectra in Fig. 1 are calculated and analyzed. The integrated section is 560 – 800 nm. The results are presented in the fourth column(Y) of Tab. 1. Comparing the results of the samples, it can be inferred that the optimal doping concentrations ranges of Bi^{3+} and Eu^{3+} are 10% – 50% and 35% – 95%, respectively.

Tab. 1 Uniform design table of nine samples, including the concentrations of Bi^{3+} and Eu^{3+} and the integrated luminous intensity, where z and k represent the concentration of ions and the serial number of ions in the uniform design, respectively

Number	$k_1(z_1)$/%	$k_2(z_2)$/%	Y
1	1(0.10)	4(57.50)	871 775
2	2(7.59)	8(107.50)	1 485 240
3	3(15.08)	3(45.00)	3 854 920
4	4(22.56)	7(95.00)	6 032 930
5	5(30.05)	2(32.50)	5 243 530
6	6(37.53)	6(82.50)	6 264 890
7	7(45.02)	1(20.00)	2 786 500
8	8(52.51)	5(70.00)	2 191 900
9	9(60.00)	9(120.00)	1 331 170

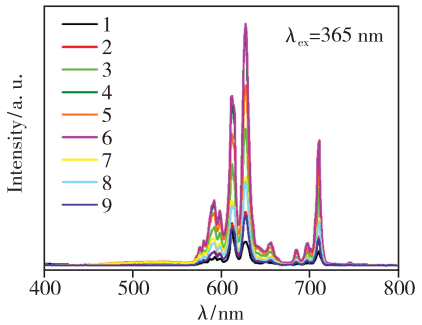

Fig. 1 Emission spectra of samples designed by uniform design(λ_{ex} = 365 nm)

3.2 Results and Test of RSM

Tab. 2 illustrates the conversion of experimental parameters between coded space and real space, where z and k represent the concentrations of ions in real space and coding space, respectively[29-30]. Thirteen samples were designed based on Tab. 2. The concentrations of Bi^{3+} and Eu^{3+} are listed in columns 3 and 4 of Tab. 3, in which the values in brackets and not in brackets represent the concentration in natural space and coding space, respectively. After thirteen samples were prepared, their PL spectra were measured. Fig. 2 presents that the luminous intensity of each sample is different. The integrated luminous intensities are calculated according to spectra, and the results are shown in the last column of Tab. 3.

Tab. 2 CCD table for concentrations of Bi^{3+} and Eu^{3+}, where z and k represent the concentrations of ions in real space and coding space, respectively

$z_j(k_j)$	$z_1(Bi^{3+})/\%$	$z_2(Eu^{3+})/\%$
$z_{2j}(r)$	50.00	95.00
$z_{0j}+\Delta_j(1)$	44.14	86.22
$z_{0j}(0)$	30.00	65.00
$z_{0j}-\Delta_j(-1)$	15.86	43.78
$z_{1j}(-r)$	10.00	35.00
$\Delta_j=(z_{2j}-z_{1j})/(2r)$	14.14	21.22
$k_j=(z_j-z_{0j}/\Delta_j$	$k_1=(z_1-30.00)/14.14$	$k_2=(z_2-65.00)/21.22$

Tab. 3 RSM table containing the concentrations of Bi^{3+} and Eu^{3+}, the corresponding samples' integrated intensity and the corresponding coefficients ($r=1.414$)

Number	k_0	$k_1(z_1)$	$k_2(z_2)$	k_1k_2	k_1^2	k_2^2	Y
1	1	1(44.14)	1(86.22)	1	1	1	4 292 510
2	1	1(44.14)	−1(43.78)	−1	1	1	4 130 000
3	1	−1(15.86)	1(86.22)	−1	1	1	4 022 890
4	1	−1(15.86)	−1(43.78)	1	1	1	3 112 560
5	1	r(50.00)	0(65.00)	0	r^2	0	3 695 560
6	1	$-r$(10.00)	0(65.00)	0	r^2	0	2 469 100
7	1	0(30.00)	r(95.00)	0	0	r^2	6 662 870
8	1	0(30.00)	$-r$(35.00)	0	0	r^2	6 459 910
9	1	0(30.00)	0(65.00)	0	0	0	6 867 920
10	1	0(30.00)	0(65.00)	0	0	0	7 766 760
11	1	0(30.00)	0(65.00)	0	0	0	7 818 470
12	1	0(30.00)	0(65.00)	0	0	0	6 987 520
13	1	0(30.00)	0(65.00)	0	0	0	8 082 376
$D_j=\Sigma x_{ij}^2$	13	8	8	4	12	12	—
$B_j=\Sigma x_{ij}y_{ij}$	72 369 820	3 021 274.44	1 359 825.44	−747 820	27 887 280	41 803 520	—
b_j	7 504 884	377 659.305	169 978.18	−186 955	−2 440 884.9	−701 355	—
S_j	2.82×10^{14}	1.14×10^{12}	2.31×10^{11}	1.40×10^{11}	4.14×10^{13}	3.42×10^{12}	—
t_j	30.96	1.97	0.89	0.69	11.87	3.41	—
α_j	0.001	0.2	0.5	0.6	0.001	0.02	—

A mathematical model, quadratic polynomial, is established based on the Tab. 3. The coefficients of each factor of the quadratic polynomial are given in the row of "b_j", and the quadratic regression equation of the coding space can be obtained as follow[30]:

$$Y = 7504884 + 377659.305k_1 + 169978.18k_2 - 186955k_1k_2 - 2440884.96k_1^2 - 701355k_2^2. \quad (1)$$

Tab. 4 shows the variance analysis of the F-test and T-test for the Eq. (1). The sum of squares and degrees of freedom can be obtained according to Tab. 4[29]. From the sum of squares and degrees of freedom, we can further judge whether the Eq. (1) is misfit and credible. The calculation is given by the following formulas:

$$F_{lf}=\frac{S_{lf}/f_{lf}}{S_e/f_e}\approx 1.813 < F_{0.25}(3,4)=2.05, \quad (2)$$

$$F_r=\frac{S_r/f_r}{S_R/f_R}\approx 22.398 > F_{0.01}(5,7)=7.46, \quad (3)$$

where F_{lf}, F_r are the loss of fitting test and the degree of confidence test, respectively. It can be seen from the test results that the Eq. (1) does not loss fitting, and the degree of confidence reaches 99%, which proves that the regression model is consistent with the actual situation[12,14,29-30]. The doping concentrations of Bi^{3+} and Eu^{3+} ions corresponding to $Y_4GeO_8:Bi^{3+},Eu^{3+}$ phosphors with the best red luminous intensity can be obtained by converting Eq. (1) to real space.

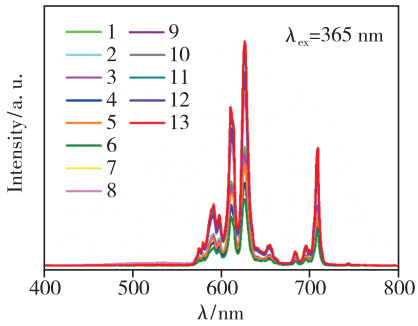

Fig. 2　Emission spectra of 13 samples in Tab. 3 designed by RSM(λ_{ex} = 365 nm)

Tab. 4　Table of variance analysis *via* T-test and F-test, in which S_R, S_r, S_{lf}, S_e and S represent the sum of residual squares, the sum of regression squares, the sum of mismatch squares, the sum of error squares and the sum of total squares, respectively

Source of variation	S_j	f	t_j	F-ratio	α_j	Significance level
k_0	2.816×10^{14}	1	30.958	—	0.001	***
k_1	1.141×10^{12}	1	1.971	—	0.2	**
k_2	2.311×10^{11}	1	0.887	—	0.5	*
k_1k_2	1.398×10^{11}	1	0.689	—	0.6	*
k_1^2	4.143×10^{13}	1	11.874	—	0.001	***
k_2^2	3.421×10^{12}	1	3.412	—	0.02	***
Residual(S_R)	2.774×10^{12}	7	—	—	—	—
Regression(S_r)	4.437×10^{13}	5	—	22.398	0.01	—
Loss of fitting(S_{lf})	1.159×10^{12}	3	—	1.813	0.25	—
Error(S_e)	1.175×10^{12}	4	—	—	—	—
Sum(S)	4.715×10^{13}	12	—	—	—	—

Notice: ***extremely significant($\alpha\leqslant0.1$), **significant($\alpha\leqslant0.3$), * relatively significant($\alpha>0.3$) ("Extremely significant" means that the existence of the term has a great impact on the Eq. (1). "Significant" means that the existence of the term has some impact on the Eq. (1). "Relatively significant" means that the term has little impact on the Eq. (1) and can be ignored).

By converting the coding space equation into natural space using the formula in Tab. 2, the binary quadratic regression equation between the doping concentration and luminescence intensity of Bi^{3+} and Eu^{3+} in natural space can be obtained. That is, replace the variable k in Eq. (1) with the variable z according to the formula in the last row of Tab. 2. The conversion result is as following:

$$Y = -12595306.02 + 799236.47z_1 + 229254.0816z_2 - 622.941z_1z_2 - 12200.69z_1^2 - 1558.097z_2^2. \quad (4)$$

According to the Eq. (4), the ions doping concentration corresponding to the sample with the strongest luminescence can be predicted by genetic algorithm. The concentrations of Bi^{3+} and Eu^{3+} of the optimal $Y_4GeO_8:Bi^{3+},Eu^{3+}$ sample (labelled as Optimal-YGO) are 31.03% and 67.36%, respectively, and the predicted strongest luminescence intensity is 7 528 268. The 3D graph of the Eq. (4) shows the

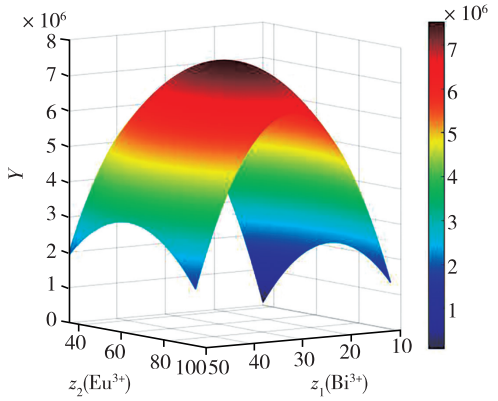

Fig. 3　The relationship between luminous intensity and concentrations of Bi^{3+}/Eu^{3+}, where z_1/z_2 represents the concentrations of Bi^{3+}/Eu^{3+} and y represents the luminous intensity.

intensity of the samples more intuitively, as indicated in Fig. 3. We can infer the relationship between the luminous intensity of samples and the concentrations of Bi^{3+}/Eu^{3+}. Obviously, when the concentration of one ion is fixed, the luminous intensity will first increase and then decrease with the increase of the concentration of another ion. As shown in the figure, it reveals that the change of concentration of Bi^{3+} has a greater impact on the luminous intensity than Eu^{3+}.

3.3 Characterization of Optimal-YGO Sample

The results of powder XRD patterns of the Optimal-YGO and the standard patterns of Y_4GeO_8 (JCPDS No. 21-1446) are presented in Fig. 4. The peaks of the sample are essentially consistent with those of the standard card, indicating that the incorporation of Bi^{3+} and Eu^{3+} has little affected the structure of the matrix, and red phosphor is successfully synthesized.

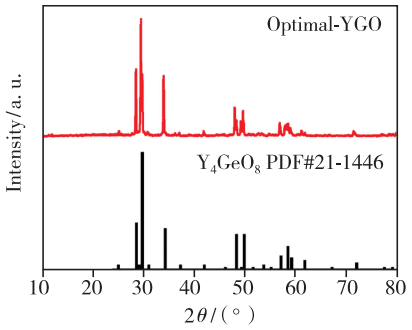

Fig. 4 XRD patterns of the Optimal-YGO and the standard card of Y_4GeO_8 (JCPDS No. 21-1446)

The PL spectra of Optimal-YGO were measured in order to further investigate its properties. Fig. 5(a) is the excitation spectra (λ_{em} = 627 nm) and the optimum excitation of the sample is 365 nm. Fig. 5(b) is the corresponding emission spectra of the sample. It can be seen that the strongest emission of the sample under the excitation of 365 nm is 627 nm. A series of emission peaks of 565 – 750 nm come from $^5D_0 \rightarrow {}^7F_J$ ($J = 0 - 4$) transitions of Eu^{3+}, respectively[31-32]. After calculation, the integral intensity of the emission spectrum is 7 520 120. Compared with the Eq. (4) simulation results, the error range is small. This proves that the RSM is highly reliable.

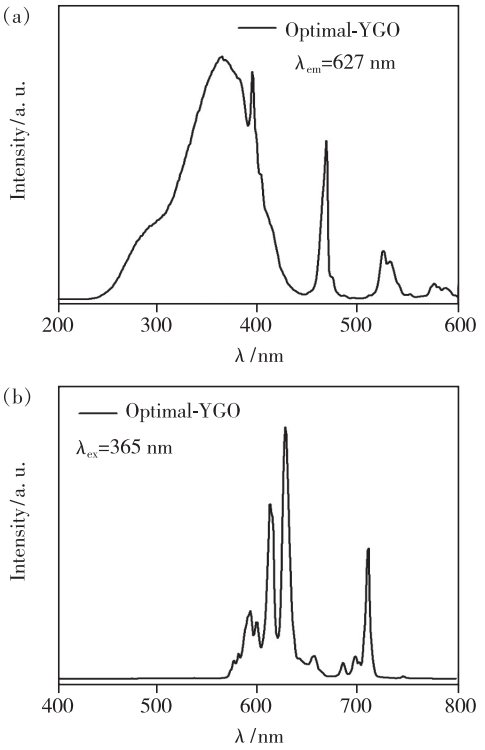

Fig. 5 (a) Excitation spectrum of Optimal-YGO (λ_{em} = 627 nm). (b) Emission spectrum of Optimal-YGO (λ_{ex} = 365 nm).

After processing the measured emission spectra data, it is concluded that the CIE of the optimal sample is (0.645 7, 0.349 0). The internal quantum efficiency (IQE) of this sample is as high as 72.5%. Tab. 5 lists some comparison results of as-prepared samples using the control variable method, and Fig. 6 shows the corresponding data[18]. The IQE, external quantum efficiency (EQE) and absorption efficiency (Abs) can be given by the following equation[33]:

$$\eta_{IQE} = \frac{\int L_S}{\int E_R - \int E_S}, \tag{5}$$

$$\eta_{EQE} = \frac{\int L_S}{\int E_R}, \tag{6}$$

$$\eta_{Abs} = \frac{\eta_{EQE}}{\eta_{IQE}}, \tag{7}$$

in which $\int L_S$ is the integral intensity of emission light with the Optimal-YGO, $\int E_S$ and $\int E_R$ are the integral intensity of exciting light with and without Optimal-YGO, respectively.

Tab. 5　Comparison of CIE, IQE, EQE and Abs of sample Y_4GeO_8: 25% Bi^{3+}, 65% Eu^{3+} and sample Optimal-YGO under 365 nm excitation, the third line is the CIE of the standard red light

	CIE(x, y)	IQE/%	EQE/%	Abs/%	Ref
Y_4GeO_8: 25% Bi^{3+}, 65% Eu^{3+}	(0.643 7, 0.349 1)	61.3	37.4	61.0	[18]
Optimal-YGO	(0.645 7, 0.349 0)	72.5	40.3	55.6	This work
Standard red light	(0.670 0, 0.330 0)	—	—	—	[11]

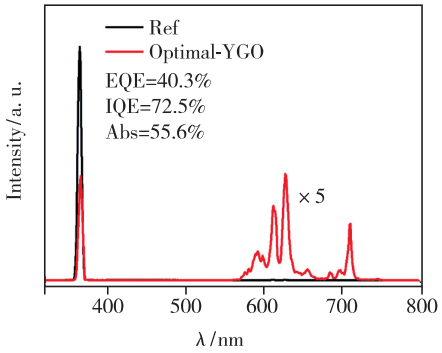

Fig. 6　The IQE, EQE and Abs of Optimal-YGO under 365 nm excitation.

The color purity (P_{color}) of the sample can be studied by the following Eq. (8) to further investigate the quality of red emission of the sample[34-35]:

$$P_{color} = \frac{\sqrt{(x - x_i) + (y - y_i)}}{\sqrt{(x_d - x_i) + (y_d - y_i)}} \times 100\% , \quad (8)$$

where (x, y), (x_i, y_i) and (x_d, y_d) represent the chromaticity coordinates of the light source under test, equal-energy reference illuminant, and dominant-wavelength point, respectively. In this work, (x, y) = (0.645 7, 0.349 0), (x_i, y_i) = (0.333, 0.333) and (x_d, y_d) = (0.650 7, 0.349 3). As a result, the color purity of YGO is about 98%, which is excellent compared with some reported phosphors, such as $Sr_3La(AlO)_3(BO_3)_4:Eu^{3+}$ (92.4%) and $Na_3Sc_2(PO_4)_3:Eu^{3+}$ (87%).

The thermal stability of the optimal sample Optimal-YGO was characterized by temperature-dependent emission spectra. Fig. 7(a) summarizes the change of the spectra of the sample with temperature. It can be seen that as the temperature rises, the sample's spectral intensity decreases. The normalization curve of the change of spectral intensity of the sample with the change of temperature is presented in Fig. 7(b). From the figure, the spectral intensity at 443 K is reduced to 50% of that at 293 K.

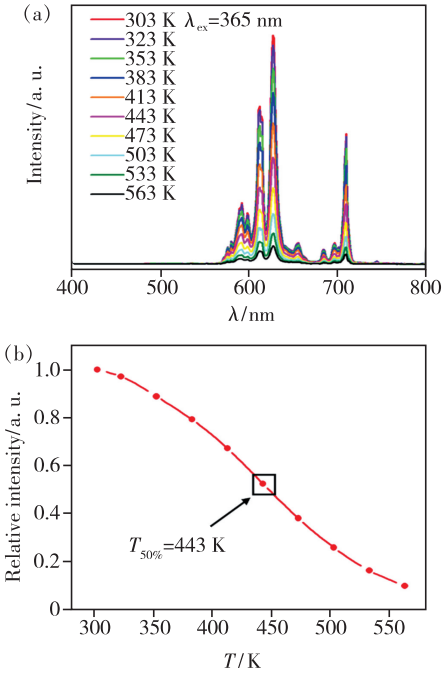

Fig. 7　(a) Temperature-dependent emission spectra of Optimal-YGO (λ_{ex} = 365 nm). (b) Normalized curve of luminous intensity with temperature.

Fig. 8 displays the change of sample color coordinates with temperature. It can be seen that the color change of the sample is not obvious with the change of temperature. The insert shows the change of specific color coordinates of the sample.

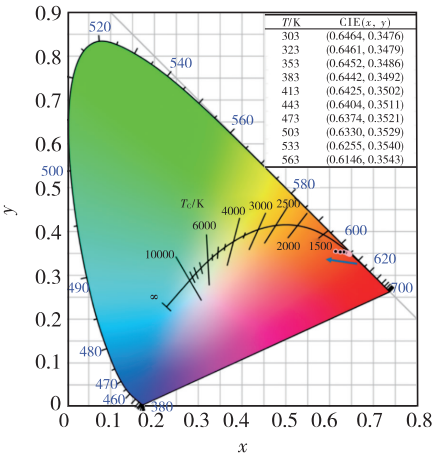

Fig. 8　CIE chromaticity diagrams of Optimal-YGO with temperature (Insert is specific data of color coordinates)

4 Conclusion

In this work, we successfully predicted the sample with the strongest luminescence through RSM more directly. The optimal concentrations of Bi^{3+} and Eu^{3+} were 31.03% and 67.36%, respectively. The optimal sample was successfully prepared. According to the measurement and calculation, the CIE of Optimal-YGO is (0.645 7, 0.349 0), the color purity is 98%, and the IQE is 72.5%. The above results not only show that Optimal-YGO has great application potential in the preparation of UV excited W-LED, but also show that RSM can predict the optimal doping contents of co-doped phosphors with the strongest luminescence.

Response Letter is available for this paper at: http://cjl.lightpublishing.cn/thesisDetails#10.37188/CJL.20220021.

References:

[1] WEI Y, XING G C, LIU K, *et al*. New strategy for designing orangish-red-emitting phosphor *via* oxygen-vacancy-induced electronic localization [J]. *Light: Sci. Appl.*, 2019, 8(1): 15-1-9.

[2] LAI S Q, ZHAO M, QIAO J W, *et al*. Data-driven photoluminescence tuning in Eu^{2+}-doped phosphors [J]. *J. Phys. Chem. Lett.*, 2020, 11(14): 5680-5685.

[3] XIANG J M, ZHENG J M, ZHOU Z W, *et al*. Enhancement of red emission and site analysis in Eu^{2+} doped new-type structure $Ba_3CaK(PO_4)_3$ for plant growth white LEDs [J]. *Chem. Eng. J.*, 2019, 356: 236-244.

[4] WU D, XIAO Y, ZHANG L L, *et al*. Highly efficient and thermally stable luminescence of $Ca_3Gd_2Si_6O_{18}:Ce^{3+},Tb^{3+}$ phosphors based on efficient energy transfer [J]. *J. Mater. Chem. C*, 2020, 8(48): 17176-17184.

[5] DANG P P, LI G G, YUN X H, *et al*. Thermally stable and highly efficient red-emitting Eu^{3+}-doped $Cs_3GdGe_3O_9$ phosphors for WLEDs: non-concentration quenching and negative thermal expansion [J]. *Light: Sci. Appl.*, 2021, 10(1): 29-1-13.

[6] ZHANG Z W, LI J H, YANG N, *et al*. A novel multi-center activated single-component white light-emitting phosphor for deep UV chip-based high color-rendering WLEDs [J]. *Chem. Eng. J.*, 2020, 390: 124601-1-10.

[7] TONG Y, CHEN Y H, CHEN S Y Z, *et al*. Luminescent properties of $Na_2GdMg_2(VO_4)_3:Eu^{3+}$ red phosphors for NUV excited pc-WLEDs [J]. *Ceram. Int.*, 2021, 47(9): 12320-12326.

[8] 章伟, 何梦婷, 乔旭升, 等. Mn^{4+}激活的典型 LED 红色荧光粉研究进展 [J]. 发光学报, 2021, 42(9): 1345-1364.
ZHANG W, HE M T, QIAO X S, *et al*. Research progress of Mn^{4+} activated typical LED red phosphors [J]. *Chin. J. Lumin.*, 2021, 42(9): 1345-1364. (in Chinese)

[9] YUE C, ZHU D C, YAN Q, *et al*. A red-emitting $Sr_3La_{(1-x)}Eu_x(AlO)_3(BO_3)_4$ phosphor with high thermal stability and color purity for near-UV-excited wLEDs [J]. *RSC Adv.*, 2019, 9(45): 26364-26372.

[10] GUO H, HUANG X Y, ZENG Y J. Synthesis and photoluminescence properties of novel highly thermal-stable red-emitting $Na_3Sc_2(PO_4)_3:Eu^{3+}$ phosphors for UV-excited white-light-emitting diodes [J]. *J. Alloys Compd.*, 2018, 741: 300-306.

[11] WANG Y, ZHAO B K, DENG B, *et al*. Spectral properties and Judd-Ofelt analysis of novel red phosphors $Gd_2InSbO_7:Eu^{3+}$ with high color purity for white LEDs [J]. *J. Rare Earths*, 2021, 39(11): 1327-1335.

[12] BABAJANI N, JAMSHIDI S. Investigation of photocatalytic malachite green degradation by iridium doped zinc oxide nanoparticles: application of response surface methodology [J]. *J. Alloys Compd.*, 2019, 782: 533-544.

[13] WANG J L, WAN W. Optimization of fermentative hydrogen production process using genetic algorithm based on neural network and response surface methodology [J]. *Int. J. Hydrogen Energy*, 2009, 34(1): 255-261.

[14] YÜCEL E, YÜCEL Y, BELELI B. Optimization of synthesis conditions of PbS thin films grown by chemical bath deposition using response surface methodology [J]. *J. Alloys Compd.*, 2015, 642: 63-69.

[15] LI J, PENG J H, GUO S H, *et al*. Application of response surface methodology (RSM) for optimization of the sintering process of preparation calcia partially stabilized zirconia (CaO-PSZ) using natural baddeleyite [J]. *J. Alloys Compd.*, 2013, 574: 504-511.

[16] LUO D H. Optimization of total polysaccharide extraction from *Dioscorea nipponica Makino* using response surface methodology and uniform design [J]. *Carbohydr. Polym.*, 2012, 90(1): 284-288.

[17] CHEN Y H, CHEN J, TONG Y, *et al.* $Y_4GeO_8:Er^{3+},Yb^{3+}$ up-conversion phosphors for optical temperature sensor based on FIR technique [J]. *J. Rare Earths*, 2021, 39(12): 1512-1519.

[18] LU Z W, ZHANG W N, CHEN J, *et al.* Tunable photoemission and energy transfer of heavily Bi^{3+}, Eu^{3+} co-doped Y_4GeO_8 phosphors [J]. *J. Lumin.*, 2021, 232: 117857.

[19] XU B B, TAN D Z, GUAN M J, *et al.* Broadband near-infrared luminescence from γ-ray irradiated bismuth-doped Y_4GeO_8 crystals [J]. *J. Electrochem. Soc.*, 2011, 158(9): G203-G206.

[20] ZHOU J C, HUANG X T, YOU J H, *et al.* Synthesis, energy transfer and multicolor luminescent property of Eu^{3+}-doped $LiCa_2Mg_2V_3O_{12}$ phosphors for warm white light-emitting diodes [J]. *Ceram. Int.*, 2019, 45(11): 13832-13837.

[21] HUANG X Y, SUN Q, DEVAKUMAR B. Preparation, crystal structure, and photoluminescence properties of high-brightness red-emitting $Ca_2LuNbO_6:Eu^{3+}$ double-perovskite phosphors for high-CRI warm-white LEDs [J]. *J. Lumin.*, 2020, 225: 117373.

[22] HUANG X Y, WANG S Y, LIANG J, *et al.* Eu^{3+}-activated Ca_2YTaO_6 double-perovskite compound: a novel highly efficient red-emitting phosphor for near-UV-excited warm w-LEDs [J]. *J. Lumin.*, 2020, 226: 117408-1-9.

[23] LI X, YANG C, LIU Q S, *et al.* Enhancement of luminescence properties of $SrAl_2Si_2O_8:Eu^{3+}$ red phosphor [J]. *Ceram. Int.*, 2020, 46(11): 17376-17382.

[24] ZHENG Z G, ZHANG J F, LIU X Y, *et al.* Luminescence and self-referenced optical temperature sensing performance in $Ca_2YZr_2Al_3O_{12}:Bi^{3+},Eu^{3+}$ phosphors [J]. *Ceram. Int.*, 2020, 46(5): 6154-6159.

[25] PENG X S, CHEN J, CHEN Y H, *et al.* Optical thermometry based fluorescence intensity ratio in $Y_2Mg_2Al_2Si_2O_{12}:Bi^{3+},Eu^{3+}$ phosphors [J]. *J. Alloys Compd.*, 2021, 885: 161010.

[26] XUE J P, YU Z K, NOH H M, *et al.* Designing multi-mode optical thermometers *via* the thermochromic $LaNbO_4:Bi^{3+}/Ln^{3+}$ (*Ln* = Eu, Tb, Dy, Sm) phosphors [J]. *Chem. Eng. J.*, 2021, 415: 128977-1-14.

[27] CAO Y X, WANG X C, DING J Y, *et al.* Constructing a single-white-light emission by finely modulating the occupancy of luminescence centers in europium-doped $(Ca_{1-x}Sr_x)_9Bi(PO_4)_7$ for WLEDs [J]. *J. Mater. Chem.* C, 2020, 8(28): 9576-9584.

[28] WANG J, PENG X S, CHENG D Z, *et al.* Tunable luminescence and energy transfer in $Y_2BaAl_4SiO_{12}:Tb^{3+},Eu^{3+}$ phosphors for solid-state lighting [J]. *J. Rare Earths*, 2021, 39(3): 284-290.

[29] LIU L J, YANG H, MA S C. Experimental study on performance of pneumatic seeding system [J]. *Int. J. Agr. Biol. Eng.*, 2016, 9(6): 84-90.

[30] FU J, YUAN H K, ZHANG D P, *et al.* Multi-objective optimization of process parameters of longitudinal axial threshing cylinder for frozen corn using RSM and NSGA-Ⅱ [J]. *Appl. Sci.*, 2020, 10(5): 1646-1-13.

[31] LI H F, ZHAO R, JIA Y L, *et al.* $Sr_{1.7}Zn_{0.3}CeO_4:Eu^{3+}$ novel red-emitting phosphors: synthesis and photoluminescence properties [J]. *ACS Appl. Mater. Interfaces*, 2014, 6(5): 3163-3169.

[32] 彭晓, 阳维维, 凌东雄, 等. 红色荧光粉 $Sr_3LiSbO_6:Eu^{3+}$ 制备及其发光性质 [J]. 发光学报, 2021, 42(4): 455-461.
PENG X, YANG W W, LING D X, *et al.* Preparation and luminescence properties of red $Sr_3LiSbO_6:Eu^{3+}$ phosphor [J]. *Chin. J. Lumin.*, 2021, 42(4): 455-461. (in Chinese)

[33] LI B, WANG S Y, SUN Q, *et al.* Novel high-brightness and thermal-stable $Ca_3Gd(AlO)_3(BO_3)_4:Eu^{3+}$ red phosphors with high colour purity for NUV-pumped white LEDs [J]. *Dyes Pigm.*, 2018, 154: 252-256.

[34] DING K, SIRU A, PANG S, *et al.* A potential red-emitting phosphor $Ca_2YTaO_6:Eu^{3+}$: luminescence properties, thermal stability and applications for white LEDs [J]. *J. Rare Earths*, 2021, 39(7): 749-756.

[35] HUA Y B, SEO Y U, KIM S Y, *et al.* Rare-earth-free $Sr_2YSb_{1-x}O_6:xMn^{4+}$: synthesis, structure, luminescence behavior, thermal stability, and applications [J]. *Chem. Eng. J.*, 2021, 412: 128633-1-13.

徐淑君(1997 –),女,安徽池州人,硕士研究生,2020 年于安庆师范大学获得学士学位,主要从事稀土离子掺杂荧光粉的制备与发光性能的研究。
E-mail: 2838110096@qq.com

郭海(1980 –),男,江西吉水人,博士,教授,博士生导师,2005 年于中国科学技术大学获得博士学位,主要从事新型稀土光学功能材料的研究。
E-mail: ghh@zjnu.cn